分类号 _____ 密级 _____

UDC _____ 编号 _____

中国科学院
博士后研究报告

不同环境活动星系核中喷流的辐射机制研究

廖能惠

合作导师 范一中 研究员

工作完成日期 2014年8月— 2016年10月

报告提交日期 2016年10月

中国科学院紫金山天文台

2016年10月

Typeset by LaTeX 2ε at October 27, 2016

With package `PostDocRep` v0.1e of CTeX.ORG

不同环境活动星系核中喷流的辐射机制研究

Radiation mechanism study on the jet of AGN in different environments

博士后姓名 廖能惠

合作导师 范一中 研究员

流动站（一级学科）名称 天文学

专　业（二级学科）名称 天体物理

研究工作起始时间 2014年8月

研究工作期满时间 2016年10月

单位名称 中国科学院紫金山天文台

报告提交日期 2016年10月

摘　　要

活动星系核中的喷流是宇宙中最剧烈的现象之一。它是研究极端环境的理想实验室，同时它也与宇宙演化密不可分。由于伽马射线光子直接携带了喷流中高能粒子的物理信息，08年发射的Fermi空间伽马射线望远镜极大的推动了本领域的发展。本文旨在利用Fermi-LAT的公开伽马射线数据，结合射电波段到X-ray的数据（包括云南天文台的2.4 m望远镜的光学数据），对伽马射线噪活动星系核特别是特殊的（新的）子类进行多波段光变研究并探寻其辐射起源，从而进一步了解喷流的形成和辐射区物理环境。我们首次发现射电中间噪度类星体（III Zw 2）也有具有产生强烈伽马射线辐射的能力。进一步分析多波段的观测数据发现其中央引擎与正常的Blazar 一致，暗示了其喷流的再活动，使得III Zw 2成为研究喷流形成和触发的理想对象。此外，我们首次发现强烈射电瓣主导的类星体（3C 275.1）的伽马射线辐射。这表明在多普勒集束效应不显著的情况下（喷流方向与视线方向夹角约20度），活动星系核能产生约10^{46} erg/s的强烈各向同性伽马射线辐射，暗示了Misaligned 源对河外伽马射线背景的贡献可能被低估了。最后，对应于新的伽马射线活动星系核子类射电平谱NLS1来说，我们首次发现了其对应的射电陡谱源（B3 1441+476）的伽马射线辐射。一方面填补了一个基于朝向的活动星系核统一模型的空白，另一方面，这个探测意味着对于RLNLS1和blazar来说，不同夹角观测到的源的数目比例不一样，暗示着伽马射线噪NLS1的实际数目显著被低估了，反之则说明这两类源的喷流结构不同。

关键词： 活动星系核，超大质量黑洞，喷流，伽马射线

Abstract

Jets in active galactic nuclei (AGN) are among the most energetic phenomena in the universe. It is an ideal laboratory for studying the extreme cosmic circumstance and tightly connected to the evolution of the universe. Since the γ rays directly trace the high energy particles in the AGN jet, Fermi space γ-ray telescope significantly improve our understanding in this domain. This report is aiming to introduce our recent studies that multiwavelength variability analyses on several "peculiar" γ-ray AGN with usage of the public LAT data as well as complementary data from radio to X rays (including photometric data observed in 2.4 meter optical telescope of Yunnan Observatories) are performed to investigate the radiation mechanism of the AGN jet in different environments and hence further probe the jet launch process as well as physical properties of the jet radiation zone. Initially, we report a discovery of γ-ray emission from a radio-intermediate quasar III Zw 2 for the first time. Further study of its multiwavelength variability properties suggests III Zw 2 harbors a recurrent activity jet, which makes it a valuable target for investigating the fueling and triggering of the activity in radio-loud active galactic nuclei. Secondly, we present the first case that γ-ray emission is detected from a strongly lobe-dominated quasar 3C 275.1 (jet viewing angle $\sim 20^{\circ}$), which provides a picture that strong γ-ray emission ($\sim 10^{46}$ erg/s) can be generated without significant Doppler boosting effect. This case suggests that the contribution of mis-aligned sources for the extragalactic γ-ray background may be underestimated. Lastly, corresponding to the flat spectra radio-loud narrow-line Seyfert I (RLNLS1) that is the new subclass of the γ-ray AGN in the Fermi era, we discovery the γ-ray emission from its large jet viewing angle counterpart, steep spectra RLNLS1 B3 1441+476, filling a blank in the orientation-based AGN unified model. Furthermore, this detection suggests that the number ratios between misaligned and aligned sources of γ-ray RLNLS1 and blazars are not even close, indicating that the number of intrinsic γ-ray RLNLS1 is highly underestimated otherwise these two types of RLAGN do

not share the same jet structure.

Keywords: Active Galactic Nuclei, Supermassive Black Hole, Relativistic Jet, Gamma Rays

目　　录

表　　格

插　　图

第一章　引言

活动星系核（AGN）作为宇宙中最强烈的稳定电磁波辐射源，一直受到天文学家的青睐。其实早在上世纪四十年代，Seyfert就注意到活动星系与正常星系的差别[1]。之后里程碑式的工作即Schmit测量到3C 273的红移[2]，导致了类星体的发现，这也是20世纪六十年代四大发现之一。随着人们对AGN的逐渐了解，现在建立了它的辐射是来自于星系中央超大质量黑洞吸积物质这样一个物理图像。正是由于活动星系核的研究，强有力的推动了黑洞物理，高能天体物理等领域的发展。另一方面，不仅仅是AGN本身，天文学家发现星系中央的黑洞质量与其核球的恒星速度弥散度存在相关关系[3, 4]，即M-σ关系，揭示了星系超大质量黑洞与其寄主星系的联系[5]。越来越多人已经意识到，AGN是探究整个宇宙演化的重要工具[6, 7]。

吸积和喷流现象在宇宙中往往被同时观测到。大约十分之一的AGN其黑洞的吸积能被转化成相对论速度运动的喷流的动能和电磁能[8]。由于这类天体相对于其他的AGN 有较强的射电辐射，所以它们被称为射电噪活动星系核（RLAGN）。AGN的喷流可以在尺度上跨越10个量级以上，并且从射电波段到甚高能伽马射线都能产生强烈的电磁波辐射[9]。考虑到如此极端的特性，RLAGN作为宇宙中最主要的高能粒子加速源之一，主导了河外伽马射线天空这也不奇怪了[10]。因此，RLAGN 是研究宇宙中高能粒子的加速、传播和辐射等非热过程的重要工具。此外它们还对研究河外伽马射线背景，河外背景光，星系际磁场及中微子背景等起了重要的作用。

因为伽马射线辐射直接携带了高能粒子的信息，所以伽马射线是研究RLAGN的重要途径。Fermi伽马射线望远镜2008年以来持续良好的运行极大地推动了本领域的发展。其搭载的LAT探测器[11]具有大的有效面积和视场，良好的空间和能量分辨率，相比于前任EGRET探测器性能有了全面的提升。良好的仪器使得探测到的伽马射线源的数目大大增加。在最新的3FGL样本中[10]，总共包括三千余个高置信度的伽马射线辐射源，其中一半左右被证认为RLAGN[12]。其中大部分的伽马射线噪AGN都是Blazar。因为它们的喷流对准我们，所以其多波段的辐射被多普勒集束效应强烈放大。Blazar其它的观测特征还有高光度，快速的光变，高度极化的光学与射电辐射及强的高能辐

射[13]。除了显著增加的伽马射线源数目，Fermi还探测到了新类型的伽马射线源。它不仅仅证实了喷流与视线夹角较大的源（射电星系和陡谱射电类星体）也具备强的伽马射线辐射能力[14]，还发现延展的射电瓣成分可以显著贡献伽马射线辐射[15]。更重要的是，Fermi还首次发现了NLS1[16]和近邻恒星形成/星暴星系[17]的伽马射线，对我们理解在不同环境下喷流的形成和伽马射线辐射机制起了很重要的帮助。此外，由于LAT的大的视场及大部分运行时间处于巡天模式的观测策略，它能够持续实时的监测整个伽马射线天空。结合地面和空间的从射电到X射线的观测，LAT能够提供一个全波段多信使的了解RLAGN的机会，这在之前的几乎不可能的。大量对RLAGN 的联测项目使得我们对喷流的传播[18]，辐射区物理性质[19, 20] 等有了进一步的认识。

虽然观测技术的进步促进了我们对RLAGN的认识，但是实际上，我们对AGN中喷流的许多基本问题还知之甚少。新的观测现象甚至带来了更多的困惑。首先喷流确切的形成机制现在还不清楚。实际上，广泛被接受的理论是喷流的强度与黑洞自旋有强烈依赖关系，但是在许多射电宁静的源里面，观测到强的X-ray的Fe Kα壳层发射线，暗示这些源的黑洞也有快速自旋。其次喷流的强度曾被认为与吸积系统的性质（倾向于在大质量黑洞低吸积率系统中被发现）有关，但是最近的伽马射线NLS1 的发现表明，在较低黑洞质量和较高吸积率系统中也能产生强烈的喷流。很令人困惑的是，从观测的角度来看，各种AGN都找到了它们自己的方法产生强烈的喷流。除了喷流的形成机制，我们对它的传播（准直），和与外界的星际介质相互作用的过程也不清楚。后者对确定喷流是否在AGN反馈中是否起了重要的作用非常关键。此外，喷流本身物理的性质，包括其物质组分和能量耗散过程等都尚不清楚。

本文旨在应用公开的Fermi-LAT的伽马射线数据，结合多波段数据，包括云南天文台的2.4 m和1 m望远镜的光学测光数据，对RLAGN进行多波段的光变研究，希望能够促进对活动星系核中喷流的理解。

第二章　Discovery of gamma-ray emission from the radio-intermediate quasar III Zw 2: violent jet activity with intraday γ-ray variability

2.1　The Radio-Loud/Radio-Quiet AGN Bimodel distribution

In optically selected samples (e.g., the Palomar-Green (PG) Quasar sample[84]), quasars with similar optical properties exhibit very different properties in radio bands[85]. The ratio of the radio flux at 5 GHz to the optical flux at B band (i.e., the radio loudness parameter $\mathcal{R} \equiv f_{5\ \mathrm{GHz}}/f_{\mathrm{B}}$) has been adopted as an indicator of the radio properties of quasars[85]. However, recent studies based on deep radio surveys, e.g., Faint Images of the Radio Sky at Twenty cm and NRAO VLA Sky Survey[86, 87], and optical massive surveys, e.g., SDSS (Sloan Digital Sky Survey) and Two Degree Field Survey[88, 89], suggest that the distribution of radio loudness of AGNs is not bimodal but rather continuous (e.g.[90, 91]). Understanding the distribution of radio loudness of AGNs is crucial for addressing the basic questions such as how jets are formed, accelerated and collimated, and why the efficiency of jet production can be so different among objects very similar in all other aspects, as well as the questions concerning jets in black hole and neutron star X-ray binaries (see review by Fender 2006[92]).

Radio-quiet AGNs, for example the Seyferts, are usually hosted by late-type galaxies with "under-luminous" or silent jets (e.g. [93]). On the other hand, it is known that radio-loud AGNs with strong radio jets almost never reside in the late type, i.e. spiral galaxies (e.g. [94], but also see [95]). Blazars, including Flat-spectrum radio quasars (FSRQs) and BL Lacertae objects, are an extreme subclass of radio-loud AGNs. They are characterized by the luminous, rapidly variable, and polarized non-thermal continuum emissions, extending from radio to γ-ray (GeV and TeV) energies, which are widely accepted to be produced in the relativistic jets oriented close to the line of sight[13, 21]. Their spectral

energy distributions (SEDs) have a universal two-bump structure in logνF$_\nu$-logν plot. The first bump is (likely) by synchrotron emission of relativistic electrons in magnetic fields while the second bump extending to γ rays is usually explained as inverse Compton (IC) scattering of soft photons from either inside and/or outside of the jet by the same population of relativistic electrons[96–99]. Besides of the typical Radio-loud quasars and Radio-quiet quasars, there are the so-called 'radio-intermediate quasars' (RIQs, [100–102]). RIQs have compact radio cores at arcsecond scales with relatively high brightness temperatures and flat and variable radio spectra in common which are similar to radio-loud quasars. However, RIQs also possess low radio-to-optical ratio and weak extended steep-spectrum emission which are atypical of radio-loud quasars. Therefore, RIQs bridge the classical radio-loud and radio-quiet AGNs and can be used to probe the connection between these two canonical groups.

III Zw 2 is a triple galaxy group. The brightest source of the group, III Zw 2A (also named as PG 0007+106 or Mrk 1501 at the redshift of $z = 0.089$, referred as III Zw 2 throughout this paper) is a AGN with Seyfert I nuclei (Zwicky 1967; Arp 1968), and also included in the PG quasar sample[84]. Its host galaxy was identified as a spiral (e.g. [105, 106]). However, recent study of the bulge/disk decomposition on its *HST* H-band image indicates an elliptical morphology[107]. An extended low surface brightness emission among the galaxy group and a tidal bridge from III Zw 2 with several knots of star forming regions linking to a nearby companion III Zw 2B suggest an undergoing merging phase[108]. Thus, considering the evidence of galaxy merging and following the morphological classification pattern of Schawinski et al. (2010)[109], we refer the host galaxy of III Zw 2 as the indeterminate-type class. III Zw 2 is famous for its large-amplitude radio variability with over 20-fold increases at timescale of years (e.g. [111]). Correlated flux variations from radio to X-rays have been observed[110]. It is also the first Seyfert with detection of superluminal jet motion (the apparent jet speed lower limit is of 1.29±0.05 c, Brunthaler et al. 2000). Other evidence of hosting strong radio jet include a core-dominated flat-spectrum radio morphology with high brightness temperature core and hard X-ray spectrum[100, 113]. However, extended radio emission of III Zw 2 is rather weak compared with its core

emission[112, 115] and its radio-loudness is moderate (from several tens to $\simeq$300, mainly due to the radio variability), which are typical behaviors of RIQs[100]. Based on the violent radio variability and its multiwavelength spectral energy distribution (SED), γ-ray emission of III Zw 2 is expected[116, 117]. Searching for the γ-ray emission of III Zw 2 both in GeV and TeV energies in the past however failed to yield significant detection[118–121].

In this work, we carry out a detailed analysis of *Fermi*-LAT γ-ray data of III Zw 2, together with our optical multi-bands photometric data observed from Yunnan Observatories and other multiwavelength data from the public data archives and the literature.

2.2 OBSERVATION and DATA ANALYSIS

2.2.1 LAT Data Analysis

Note that the recently released Pass 8 data set has been significantly improved in comparison with the former ones, including a wide energy reach (changing from the range of 0.1-300 GeV to 60 MeV-500 GeV), an enhanced effective area especially in the low energy range, and the better localization. All these lead to an improvement of 30%-50% enhanced differential point-source sensitivity[122]. So the Pass 8 LAT data of III Zw 2 have been used. Since the LAT data analysis process is similar with it that is adopted in 3C 275.1, it is not detailedly introduced here.

2.2.2 Swift Data Analysis

Since 2007, the space X-ray mission, *Swift*[123] has observed the source region 9 times. We excluded the observation taking on 2010 February 2 (Obs ID = 00036363004) because of too short exposure ($\sim$ 75 s). When available, we analyzed both XRT and UVOT data with the FTOOLS software version 6.17. For XRT data, we performed the initial event cleaning with `xrtpipeline` using standard quality cuts, and then extracted the source spectra within circular regions with a radius of 20 pixels. The ancillary matrix files produced by the task `xrtmkarf` and the response matrix files (v012) were used for spectral analysis.

We also grouped the spectra to have at least 20 counts per bin to ensure valid results using χ^2 statistical analysis. By linking the value of the hydrogen column density, we fitted the left 8 observational data sets simultaneously by an absorbed power-law model and sumamrize the results in Table2.1. The parameter of absorption (nH = $3.96^{+2.23}_{-2.22}$ $\times 10^{20}$ cm^{-2}) is consistent with the values given by the data from other X-ray missions (e.g. [110]). The UVOT has six filters: V, B, U, UVW1, UVM2, and UW2 with a coverage of 2.1−7.8 eV. We performed aperture photometry using `uvotsource` with a 5 arcsec circular aperture, and the background extraction was carried out in a larger source free region.

表 2.1: *Swift* Results

ObsID	Date	Γ_X	F_X	*V*	*UW1*	*UM2*	*UW2*
00036363001	2007-06-21	$1.60^{+0.11}_{-0.10}$	$1.11^{+0.08}_{-0.08}$	...	...	...	...
00036363002	2009-05-22	$1.66^{+0.10}_{-0.10}$	$1.11^{+0.08}_{-0.08}$	...	...	...	...
00036363003	2009-09-03	$1.98^{+0.84}_{-0.69}$	$1.08^{+0.49}_{-0.27}$	...	...	...	...
00036363005	2010-02-07	$1.69^{+0.10}_{-0.09}$	$1.08^{+0.07}_{-0.07}$	...	...	...	...
00036363006	2010-07-08	$1.55^{+0.15}_{-0.14}$	$1.80^{+0.21}_{-0.21}$	3.68 ± 0.09	2.09 ± 0.05	1.62 ± 0.03	1.65 ± 0.03
00036363007	2010-07-08	$1.64^{+0.12}_{-0.11}$	$1.77^{+0.14}_{-0.14}$	...	...	...	1.63 ± 0.03
00036363008	2012-01-03	$1.64^{+0.14}_{-0.14}$	$0.72^{+0.08}_{-0.08}$	2.07 ± 0.06	0.73 ± 0.02	0.57 ± 0.03	0.54 ± 0.01
00049402001	2013-05-16	$1.43^{+0.33}_{-0.31}$	$1.42^{+0.39}_{-0.34}$	...	1.21 ± 0.02	0.94 ± 0.02	0.95 ± 0.02

Note: The absorption column density for estimation of X-ray flux is constrained as $3.96^{+2.23}_{-2.22} \times 10^{20}$ cm^{-2}, with χ^2/dof of 211.0/216.Unabsorbed 0.5−10 keV X-ray fluxes are in units of 10^{-11} erg cm^{-2} s^{-1}. The extinction magnitudes in four UVOT bands are calculated as: $A_V = 0.275$, $A_{UW1} = 0.582$, $A_{UM2} = 0.820$, $A_{UW2} = 0.718$. The absorption corrected optical/UV fluxes are in unit of mJy.

2.2.3 Optical Observation and Data Analysis

The variability of III Zw 2 was photometrically monitored in optical bands at Yunnan Observatories, making use of the 2.4 m telescope [1] and the 1.02 m telescope [2]. Details about these telescopes have been introduced in[20]. The standard differential photometric procedure was followed. Sky flat field at dusk and dawn in good weather conditions and bias frames were taken at every observing night. Different exposure times were applied for various seeing and weather conditions. All frames were processed using bias and flat-field corrections by the task `CCDRED` package of the `IRAF` software, and the photometry was performed by the `APPHOT` package. Magnitudes of the source were calculated by with calibration

[1] http://www.gmg.org.cn

[2] http://www1.ynao.ac.cn/∼omt/

stars in the image frame [3]. Observing uncertainty of every night was the root-mean-square (RMS) error of differential magnitude between two calibration stars. At least one of them must be fainter than or as bright as the source[124, 125]. The multi-band magnitudes observed from Yunnan Observatories are listed in Table2.2.

表 2.2: The multi-bands photometric data from Yunnan Observatories[a]

MJD[b]	Mag[c]	SigMag[d]	Band[e]
54373.71	14.58	0.09	I
54400.63	14.70	0.03	I

Note: [a] A portion is shown here for guidance regarding its form and content. The full table is available in its entirety in machine-readable forms in the online journal. [b] The observation date. [c] The nightly average magnitude. The correction for the interstellar extinction has been already completed. [d] Uncertainty of magnitude. [e] The photometric band.

Complementary optical data were derived from the Catalina Real-time Transient Survey (CRTS[126, 127]). The photometry was transformed from the unfiltered instrumental magnitude to Cousins V by $V = V_{CSS} + 0.31(B-V)^2 + 0.04$ [4]. We averaged the values obtained during the same observing night. The CRTS daily light curve starts from MJD 53706 to MJD 56223 with 94 data points, nearly one observation per month, performing a well coverage at timescale of years. The correction for the interstellar extinction and the color excess of the observed optical/UV magnitudes were adopted[128, 129]. And optical photometric data were converted from magnitude system to flux in Jansky[130]. Consistence between different optical observation systems was checked. Note that the CRTS fluxes tend to be systematically higher than fluxes from others. For example, an UVOT observation at MJD 55929.5 gave a V band flux density of 2.1 mJy while a CRTS observation at MJD 55930.1 provided a V band flux density of 4.1 mJy. Since III Zw 2 was then at optical low state, such a discrepancy could not be caused by intrinsic variability. Thus, the CRTS light curve was only used for the purpose of exhibition of long timescale variability trend.

[3] https://www.lsw.uni-heidelberg.de/projects/extragalactic/charts/
[4] http://nesssi.cacr.caltech.edu/DataRelease/FAQ2.html#improve

2.2.4 Radio Data

III Zw 2 is included in the Owens Valley Radio Observatory (OVRO) 40 m telescope monitoring program[5]. This program encompasses over 1500 objects above declination of 20°, most of which are blazars, with observations for each source twice per week at a frequency of 15 GHz[131]. III Zw 2 is also included in the Monitoring of Jets in Active Galactic Nuclei With VLBA Experiments (MOJAVE[6]) program[132], from which multi-epoch VLBA observations at 15 GHz of several hundreds of the brightest, most compact radio sources in the northern sky have been carried out. Recently, radio data of III Zw 2 from the MOJAVE program have been published, including core and jet light curves as well as jet motion features[133].

2.3 RESULTS

2.3.1 Detecting significant gamma-ray emission from III Zw 2

We initially perform a fit to the entire 7-year *Fermi*-LAT data and do not find a significant γ-ray source in the direction of III Zw 2. For the `unbinned` likelihood analysis, the TS value of the presumed γ-ray source is only $\simeq$15 ($< 4\sigma$), as shown in Figure2.1, consistent with its absence in any γ-ray source catalogs. For the tentative gamma-ray emission, a photon flux of $(6.6\pm2.1)\times10^{-9}$ ph cm^{-2} s^{-1} and a photon index of 3.0±0.3 are obtained (we refer to a spectral index α as the energy index such that $F_\nu \propto \nu^{-\alpha}$, corresponding to a photon index $\Gamma_{\rm ph} = \alpha + 1$). And the corresponding isotropic γ-ray luminosity in the range from 100 MeV to 500 GeV is $(4.6\pm1.3)\times10^{43}$ erg s^{-1} (throughout this paper we adopt a ΛCDM cosmology model with $H_0 = 67$ km s^{-1}Mpc^{-1}, $\Omega_m = 0.32$, $\Omega_\Lambda = 0.68$[59]).

We then search for possible short-term γ-ray outburst. Firstly, the year-bin γ-ray light curve is extracted (see Figure2.2). Except for the second and sixth bins, the TS values of the emission in other time bins are below 1. The TS value of the emission in the sixth time bin is also relatively low, which is $\simeq$6 (i.e., $< 3\sigma$). However, the TS value of the γ-ray emission in the second time

[5]http://www.astro.caltech.edu/ovroblazars/
[6]http://www.physics.purdue.edu/astro/MOJAVE/index.html

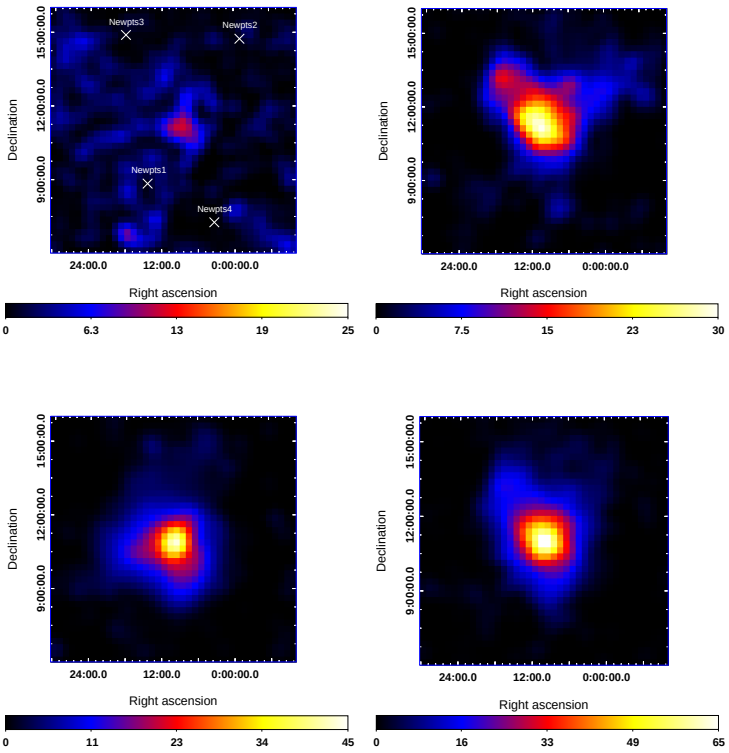

图 2.1: TS map of photons from 100 MeV to 500 GeV for $10^\circ \times 10^\circ$ region centered at III Zw 2. Upper left panel is for the entire 7-year LAT data; upper right panel represents to γ-ray flare in Nov. 2009 and bottom left is for another flare in May 2010; bottom right is for the joint analysis.

bin is as high as 38 ($> 5\sigma$). We also extract monthly γ-ray light curve for the whole 7 years LAT data. Except for the second year LAT data, the highest TS value of the monthly bin is about 5, so III Zw 2 has not been detected during most of the LAT observational time. The rather weak signal appears in the sixth year LAT data is likely due to the background fluctuation. On the other hands, two γ-ray flares have been identified in the monthly γ-ray light curve in the second year Fermi-LAT data. Then further the 2 days time bin γ-ray light curves are extracted during these two periods. The start and end of the two flaring epochs are selected as from MJD 55120 to MJD 55190, and MJD 55322 to MJD 55368, respectively. Individual `gtlike` analyses for these two epochs

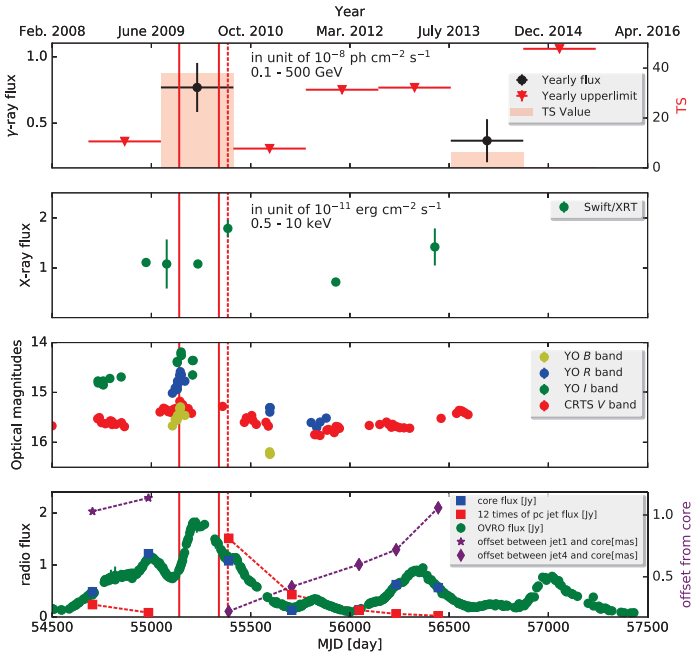

图 2.2: The multiwavelength light curves of III Zw 2. In the optical panel, green, blue and yellow circles are the magnitudes of I, R and B bands observed in Yunnan Observatories (YO), respectively. The red circle are CRTS V band magnitudes plus 0.8 mag. The two solid red vertical lines mark the peaking times of the two γ-ray flare and the dashed red vertical line respond to the time of the simultaneous *Planck*, *Swift*, and *Fermi* campaign.

give the TS values of 35.3 and 50.9, respectively. Such significant signals are confirmed by the TS maps, see Figure2.1. Since III Zw 2 is a high Galactic latitude source ($|l| > 50°$), contamination from uncertainty of Galactic diffuse emission is negligible. And during such short time periods, the newly emerging γ-ray source is one of the most dominate source within the ROI. The only source with comparable γ-ray photon flux is $> 7°$ away. We hence conclude that the detection of γ-ray emission is robust. Furthermore, localization of the central excess is performed. The γ-ray position of R.A. 2.621° and decl. 11.1232° is obtained for the flare in 2009, and R.A. 2.440° and decl. 10.9349° is for the other